Original Article

Novel fat suppression technique for ultrashort echo time MRI using single-point Dixon phase modeling

Nathan Newbury[1#], Sam Sedaghat[2#], Jiyo S. Athertya[1], Soo Hyun Shin[1], Yajun Ma[1], Saeed Jerban[1], Michael Carl[3], Melissa Lou Silva[1], Eric Y. Chang[1,4], Jiang Du[1,5,6], Hyungseok Jang[7]

[1]Department of Radiology, University of California, San Diego, San Diego, CA, USA; [2]Department of Diagnostic and Interventional Radiology, University Hospital Heidelberg, Heidelberg, Germany; [3]GE Healthcare, San Diego, CA, USA; [4]Radiology Service, Veterans Affairs San Diego Healthcare System, San Diego, CA, USA; [5]Research Service, Veterans Affairs San Diego Healthcare System, San Diego, CA, USA; [6]Department of Bioengineering, University of California, San Diego, San Diego, CA, USA; [7]Department of Radiology, University of California, Davis, Sacramento, CA, USA

Contributions: (I) Conception and design: N Newbury, S Sedaghat, J Du, H Jang; (II) Administrative support: JS Athertya, SH Shin, Y Ma, J Du, H Jang; (III) Provision of study materials or patients: S Sedaghat, S Jerban, ML Silva, EY Chang, H Jang; (IV) Collection and assembly of data: N Newbury, JS Athertya, SH Shin, Y Ma, S Jerban, M Carl, H Jang; (V) Data analysis and interpretation: N Newbury, S Sedaghat, H Jang; (VI) Manuscript writing: All authors; (VII) Final approval of manuscript: All authors.

[#]These authors contributed equally to this work.

Correspondence to: Hyungseok Jang, PhD. Department of Radiology, University of California, Davis, 4860 Y Street, Suite 3100, Sacramento, CA 95817, USA. Email: hyjang@ucdavis.edu.

Background: Fat suppression plays a vital role in numerous magnetic resonance imaging (MRI) examinations, particularly in the musculoskeletal (MSK) system. However, current fat suppression methods are not fully optimized for ultrashort echo time (UTE) imaging, despite being essential for many advanced UTE-based imaging applications. This study aimed to investigate a novel fat suppression technique for UTE MRI using a single-point Dixon (1p-Dixon) approach through phase modeling.

Methods: In this study, four cadaveric human knee joints, and six healthy volunteers were included. A 1p-Dixon-based fat suppression method was developed, which utilizes intrinsic information from complex UTE signals. Additionally, a data-driven approach based on the phase distribution was used for the decomposition of water and fat signals in short T2 tissues. The feasibility of the proposed method was evaluated in a fat-water phantom first and validated in *ex vivo* and *in vivo* human knee joints. The patella tendon, cartilage, posterior cruciate ligament (PCL), anterior cruciate ligament (ACL), and meniscus were evaluated in each knee.

Results: In the phantom experiment, there was a significant correlation between the estimated fat fraction and the actual fat fraction ($R>0.98$; $P<0.05$). The *ex vivo* experiment revealed a significant difference in contrast-to-noise ratios (CNRs) measured from the two images without and with 1p-Dixon ($P<0.001$). The CNR values ranged from 3.4±0.5 to 9.6±5.0 and 1.8±1.6 to 4.1±0.8 for measurement with and without 1p-Dixon, respectively. The 1p-Dixon significantly improved the contrast in the *in vivo* experiment ($P<0.0001$). The CNR values ranged from 5.1±6.0 to 41.0±9.7 and 2.7±1.2 to 15.4±3.3 for measurement with and without 1p-Dixon, respectively in the *in vivo* experiment.

Conclusions: Our novel fat suppression technique has been shown to provide a fast, time-saving, and robust fat suppression for UTE imaging without the need for additional scans.

Keywords: Ultrashort echo time (UTE); fat suppression; Dixon; musculoskeletal (MSK); knee

Submitted Sep 20, 2024. Accepted for publication Feb 27, 2025. Published online Apr 10, 2025.
doi: 10.21037/qims-24-1998
View this article at: https://dx.doi.org/10.21037/qims-24-1998

Introduction

Ultrashort echo time (UTE) imaging has been extensively investigated for musculoskeletal (MSK) imaging (1-4). Many tissues within the MSK system have short T2 relaxation times that are invisible in conventional magnetic resonance imaging (MRI) (5). Short T2 tissues are not limited to the MSK system but are delineated in many parts of the body, such as the lungs (6) and the human brain (7-10).

Fat suppression is crucial in many MRI examinations, especially in the MSK system (11-15). For UTE imaging, the existing fat suppression techniques are suboptimal, although, in state-of-the-art UTE techniques, fat suppression is mandatory for many imaging examinations (1,16). For example, conventional fat-saturation may attenuate the partial signal of the short T2 tissues, and a two-point Dixon (2p-Dixon) method can misestimate the fat and water signal (17,18). Multi-point Dixon (mp-Dixon) techniques are also feasible techniques for fat suppression in UTE imaging (13). However, the mp-Dixon techniques need multiple images at short and long TEs, which may impose a longer scan time.

As a breakthrough, the single-point Dixon (1p-Dixon) has been investigated in UTE imaging and has shown feasibility in successfully suppressing fat without affecting signal from short T2 tissues (18-20). Initially proposed 1p-Dixon UTE imaging is based on indirect estimation of fat signal at a later TE, which requires additional image acquisition to compensate for B0 inhomogeneity (18,19). Recently, 1p-Dixon UTE imaging has been demonstrated in spine imaging, which is based on direct fat estimation at UTE (20). In this method, an iterative decomposition is performed to estimate phase error as well as fat and water signals, with the underlying assumption that B0 inhomogeneity-induced phase error is negligibly small and smooth. B1 phase (i.e., initial phase offset) is also known to be smooth. However, this approach requires a complicated process with manual parameter tuning.

Another challenge is that 1p-Dixon requires ground truth about the off-resonant fat phase to decompose a complex magnetic resonance (MR) signal into water and fat components. This information is typically obtained by calibrating the fat phase with the given effective echo time (TE) (18,21) in an additional scan, as analytically found fat phase can be erroneous due to ambiguous effective TE (22). In this study, we evaluate a simple, time-saving, and robust data-driven 1p-Dixon UTE imaging approach. The feasibility and efficacy of the proposed approach will be demonstrated in the phantom model, in *ex vivo* cadaveric human knee samples, and in healthy volunteers. We present this article in accordance with the STROBE reporting checklist (available at https://qims.amegroups.com/article/view/10.21037/qims-24-1998/rc).

Methods

Imaging subjects

A fat-water phantom was made using pure peanut oil and lard, whose chemical composition is known to be similar to the fat in the human body. The phantom was made with agarose gel (2%) molded into a cylindrical plastic container. Smaller tubes were prepared using a mixture of detergents (0.5% Triton X-100, 0.5% Tween-20, and 0.5% SDS) and six different concentrations (0%, 10%, 20%, 40%, 60%, and 100%) of peanut oil and lard (i.e., two sets of six tubes) and embedded in the container filled with agarose gel.

Additionally, cadaveric and *in vivo* human knee joints were included in this study to demonstrate the feasibility and efficacy of the proposed 1p-Dixon UTE imaging. Four cadaveric human knee joints were procured from the National Disease Research Interchange. The knee joints were snap-frozen postmortem. The frozen knee joints were completely thawed prior to MRI. The 1p-Dixon method was further tested in healthy volunteers (six females, 41±15 years old, *Table 1*). This study was conducted in accordance with the Declaration of Helsinki (as revised in 2013). The *in vivo* experiment was approved by the Human Research Protections Program (HRPP) of the University of California, San Diego (No. 201909). Written informed consent was obtained from the study participants.

1p-Dixon

1p-Dixon decomposes the measured complex MRI signal, $S_{exp,}$ into a water and fat signal. S_{exp} can be modeled as:

Table 1 Demographic information of the healthy volunteers (*in vivo*)

Parameters	Data (n=6)
Sex	
Female	6
Male	0
Age (years)	41±15

Data are presented as number or mean ± standard deviation.

$$S_{\exp} = \left(W + Fe^{i\theta(TE)}\right)e^{i\varphi} \quad [1]$$

where W and F are the magnitudes of the water and fat signals, $\theta(TE)$ denotes the phase evolution at a given TE due to chemical shift of fat, and ϕ denotes additional phase error due to B1 phase and B0 field inhomogeneity. The B1 phase is generally known to be smooth, and the phase error induced by B0 inhomogeneity is also smooth at an ultrashort TE (<0.1 ms) due to the small phase evolution. Therefore, ϕ can be assumed to be smooth in UTE imaging. Once the phase error, ϕ, is corrected as $S = S_{exp} * e^{-i\phi}$, the resultant complex signal, S, can be directly decomposed to water and fat with a known $\theta(TE)$ by using the following equations.

$$F = \frac{\mathrm{Im}(S)}{\sin\left(\theta(TE)\right)} \quad [2]$$

$$W = \mathrm{Re}(S) - F\cos\left(\theta(TE)\right) \quad [3]$$

where *Im* and *Re* are the operators to take imaginary and real parts in the complex signal, and W and F represent water and fat signals, respectively.

Theoretically, the phase term caused by the chemical shift of fat, $\theta(TE)$, can be modeled with known off-resonant multiple fat peaks, which is unfortunately challenging due to ambiguous effective TE resulting from system imperfections and eddy current effect in UTE imaging. As an alternative, we propose a data-driven approach to estimate ϕ and $\theta(TE)$, which utilizes the phase information from the single UTE image itself without the need for additional information.

Phase modeling of ϕ and θ(TE)

Masking out the voxels with pure background noise or with a low signal-to-noise ratio (SNR) is an important step for robust phase processing. *Figure 1* demonstrates an example of the generation of a mask.

B1 and B0 field-induced phase error, ϕ, can be modeled as a low-order polynomial fitted to the phase of the measured signal, $\angle S_{exp}$, under the assumption of spatial smoothness, as shown in Eq. [4].

$$\phi(x,y,z) = \sum_{k=0}^{3}\sum_{j=0}^{3-k}\sum_{i=0}^{3-j-k} C_{ijk}x^i y^i z^k + \sum_{n=0}^{4} C_{n4}x^i y^{4-i} \quad [4]$$

where C represents all coefficients to be minimized and x, y, z represent spatial voxel dimensions. Note that the global three-dimensional (3D) phase image was utilized for the fitting of the 3D polynomial.

After correction of ϕ, the resultant complex UTE image is further processed to determine $\theta(TE)$ (i.e., fat-induced phase), by using a data-driven approach based on the histogram of the phase distribution. In this study, every voxel in the bottom 2.5% of the phase distribution was identified as pure water and capped to a minimum phase taken as the value of the 2.5 percentile. Every voxel in the top 2.5% of the distribution was identified as pure fat and capped to a maximum phase taken as the value of the 97.5 percentile. All phase values were zeroed by the minimum phase to remove the constant phase offset added in the UTE phase data and hence set the water phase to zero.

Data processing

Image reconstruction was performed using the Berkeley Advanced Reconstruction Toolbox (23). The reconstructed images with data acquired by individual receive channels were combined to form a complex image (24). The phase map from S_{exp} was unwrapped using a 3D unwrapping algorithm provided by the FMRIB Software Library (v5.0) (25). After correction of ϕ and tuning of $\theta(TE)$, the phase image was processed with 1p-Dixon fat and water separation based on Eq. [2] and Eq. [3].

MRI

A 3D UTE sequence based on cones trajectory was utilized (26), which was implemented in a 3T clinical MR scanner (MR750, GE Healthcare, Milwaukee, WI, USA). *Figure 2* shows the pulse sequence diagram and k-space trajectory.

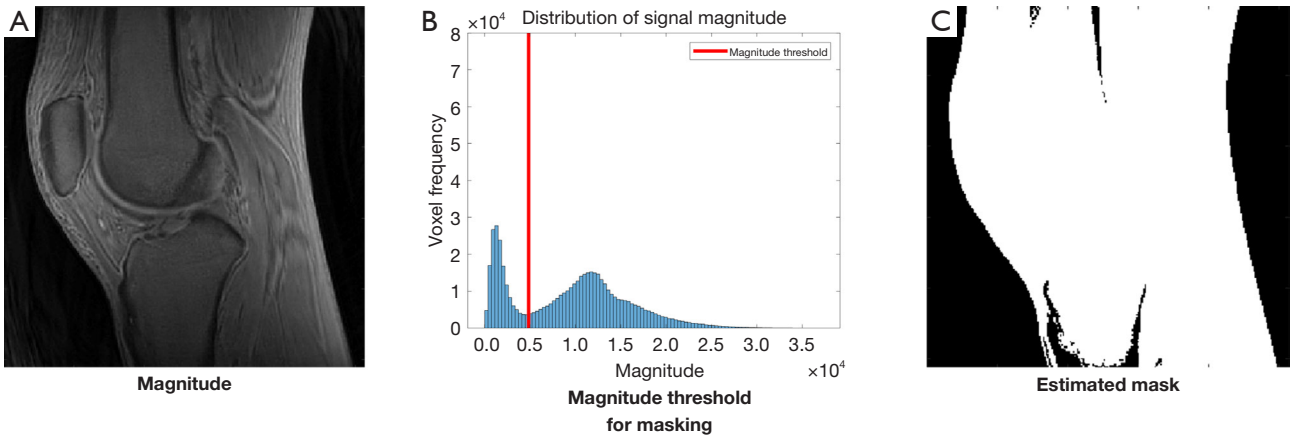

Figure 1 Mask generation based on the histogram of the image. (A) An input UTE image; (B) signal histogram; (C) generated mask. UTE, ultrashort echo time.

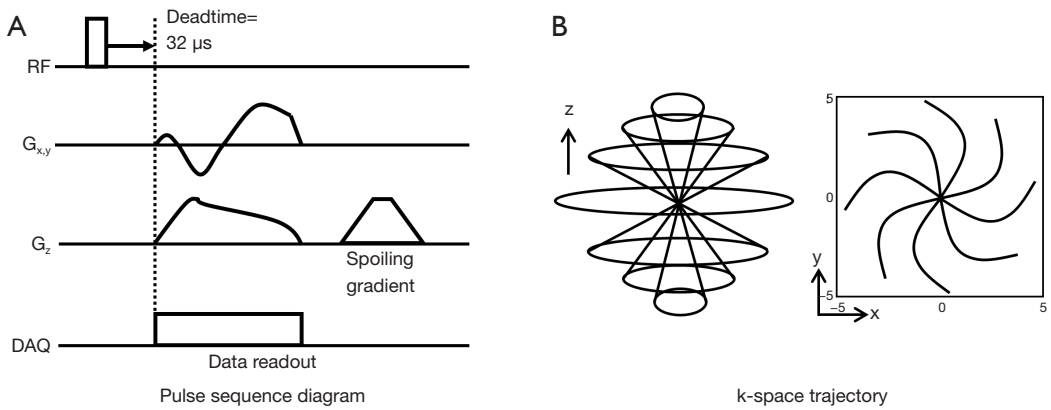

Figure 2 3D UTE cones imaging. (A) Pulse sequence diagram; (B) the k-space trajectory. 3D, three-dimensional; DAQ, data acquisition; RF, radiofrequency; UTE, ultrashort echo time.

3D UTE MRI was performed using an 8-ch transmit/receive knee coil (GE Healthcare) and the following imaging parameters: (I) fat phantom: repetition time (TR) =20 ms, nominal TE =32 μs, a flip angle (FA) =10°, field of view (FOV) = 120×120×114 mm^3, matrix size =192×192×38, readout bandwidth (rBW) =167 kHz, the number of spokes =11,200, and a scan time =224 seconds; (II) *ex vivo* knee: TR =20 ms, nominal TE =32 μs, FA =10°, FOV =150×150×84 mm^3, matrix size =256×256×42, rBW =125 kHz, the number of spokes =14,550, and a scan time =291 seconds; (III) *in vivo* knee: TR =20 ms, nominal TE =32 μs, FA =5°, FOV =150×150×96 mm^3, matrix size =256×256×32, rBW =125 kHz, the number of spokes =6,150, and a scan time =123 seconds. For comparison, one volunteer underwent additional imaging using fat-saturation, 2p-Dixon with TEs of 0 and 3.3 ms, and conventional 1p-Dixon with TEs of 0 and 2.7 ms, with all other imaging parameters kept consistent.

Statistics

Contrast-to-noise ratios (CNRs) were calculated for the patella tendon, cartilage, posterior cruciate ligament (PCL), anterior cruciate ligament (ACL), and meniscus. Descriptive statistics were used where appropriate. To compare group values, the *t*-test and Mann-Whitney *U* test were used. Correlations were determined using the Pearson's correlation (R). P values <0.05 were rated as significant.

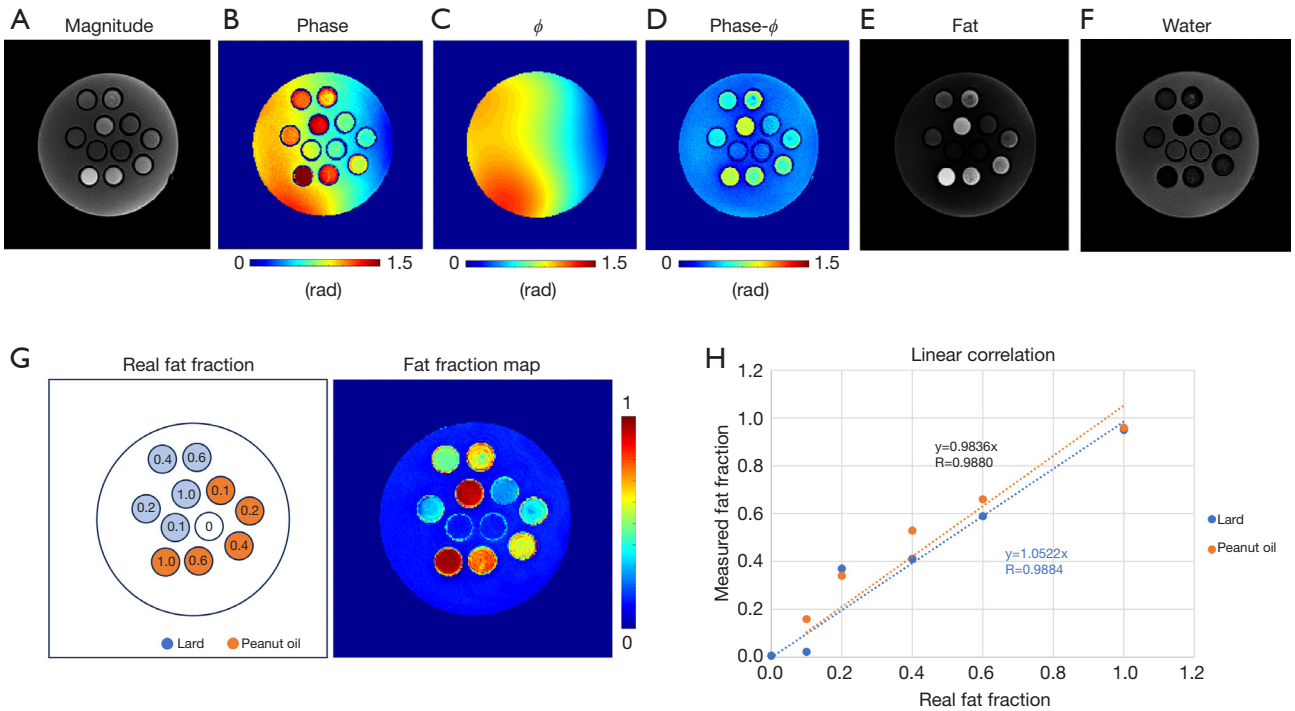

Figure 3 A fat-water phantom. (A) The magnitude and (B) phase of the input UTE image; (C) the estimated ϕ map from 3D surface modeling with polynomial fitting; (D) ϕ-corrected phase image; the resultant (E) fat and (F) water images from 1p-Dixon; (G) real and estimated fat fractions; (H) the linear correlation. 1p-Dixon, single-point Dixon; 3D, three-dimensional; UTE, ultrashort echo time.

Results

Phantom experiment

Figure 3 shows the results from the phantom experiment. After correction of ϕ, 1p-Dixon yielded reliable fat and water separation with the estimated $\theta(TE)$. The estimated fat fraction showed a significantly high linearity with respect to the actual fat fraction. Accordingly, the R was higher than 0.98 (P<0.05; *Figure 3H*).

Ex vivo experiment

Figure 4 demonstrates the phase modeling and correction process. In *Figure 4A*, the raw phase is fitted to Eq. [4] to find an estimate of the phase error, ϕ. *Figure 4B* shows line profiles before and after ϕ is subtracted out. *Figure 4C* shows the corrected signal phase distribution and the phase error offset and $\theta(TE)$ cap. *Figure 4D* shows the resultant phase of the UTE image after phase correction of ϕ and removal of the constant phase offset.

Figure 5 shows representative slices from all four cadaveric knee specimens, where robust fat suppression was achieved without noticeable impacts on the signal from short T2 tissues. *Table 2* shows the CNR between tissues of interest and neighboring tissues for the magnitude image and the 1p-Dixon estimated water image of the cadaveric knees. A significant difference in the CNRs measured from the two images without and with 1p-Dixon was found (P=0.0002). The CNR values ranged from 3.4±0.5 to 9.6±5.0 and 1.8±1.6 to 4.1±0.8 for measurement with and without 1p-Dixon, respectively. The 1p-Dixon worked well for the patella tendon, cartilage, PCL, and ACL, while there was no significant difference regarding the meniscus.

In vivo experiment

Figure 6 shows the results from four representative healthy volunteers. In the estimated water images, short and long T2 tissues of interest are clearly delineated, including tendons (yellow arrows), ligaments (red arrows), muscles (green arrows), and cartilages (blue arrows). *Table 2* shows the CNR between tissues of interest and neighboring tissues for the magnitude image and the 1p-Dixon estimated

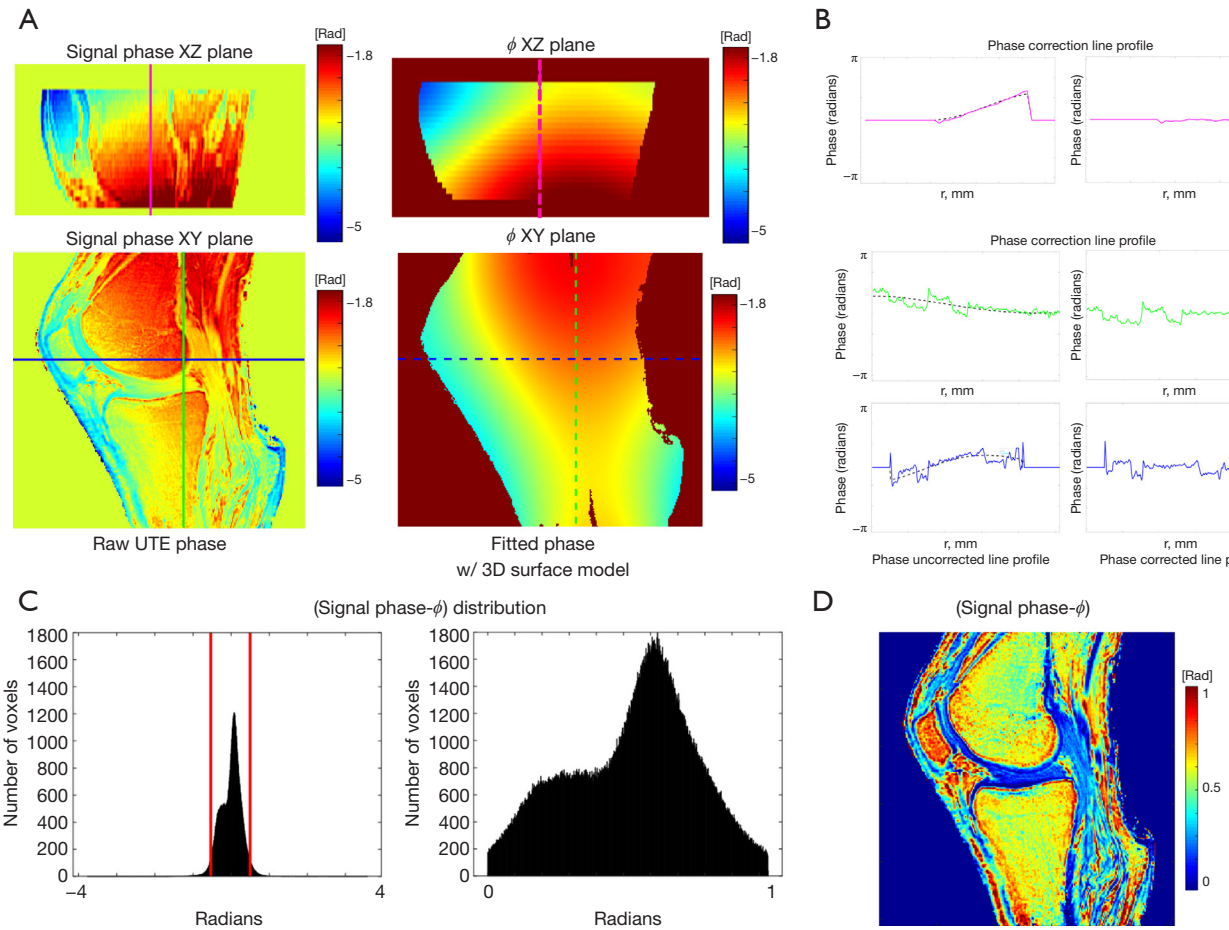

Figure 4 3D phase modeling of ϕ for 1p-Dixon in an *ex vivo* knee joint. (A) The raw phase from the UTE image and the fitted surface model; (B) the line profiles; (C) the phase distribution after ϕ-correction (before or after capping outliers); (D) the resultant phase of the ϕ-corrected image. The phase-corrected complex image is input to the subsequent 1p-Dixon process. 1p-Dixon, single-point Dixon; 3D, three-dimensional; UTE, ultrashort echo time; w/, with.

water image from the six healthy volunteers. In all regions of interest from the six healthy volunteers, 1p-Dixon significantly improved the contrast (P<0.0001). The CNR values ranged from 5.1±6.0 to 41.0±9.7 and 2.7±1.2 to 15.4±3.3 for measurement with and without 1p-Dixon, respectively. The 1p-Dixon worked well for all investigated short T2 tissues, while again, the meniscus showed the lowest difference between the measurements with and without 1p-Dixon. Accordingly, the *in vivo* experiment was revealed to be more robust than the *ex vivo* experiment regarding CNR.

Figure 7 compares fat-saturation, 2p-Dixon, conventional 1p-Dixon, and the proposed 1p-Dixon with phase modeling in a healthy volunteer. Fat-saturation does not provide a fat fraction since no fat image is acquired, while the conventional 1p-Dixon provides the fat fraction at the second TE (2.7 ms), where fat separation is performed. Both fat-saturation and the proposed 1p-Dixon with phase modeling provided real signal at the ultrashort TE, whereas the conventional 2p-Dixon generated the water image by synthesizing two images acquired at different TEs. The conventional 1p-Dixon water image was obtained by scaling the fat signal to compensate for the signal decay of fat estimated at TE =2.7 ms, thereby indirectly estimating the water signal at the ultrashort TE. Overall, all methods achieved effective suppression of fat in the bone marrow and fat pad. Importantly, the proposed 1p-Dixon with phase modeling delineated small structures of short T2 tissues more effectively than the other methods (red arrows), likely due to its capability for direct signal detection and

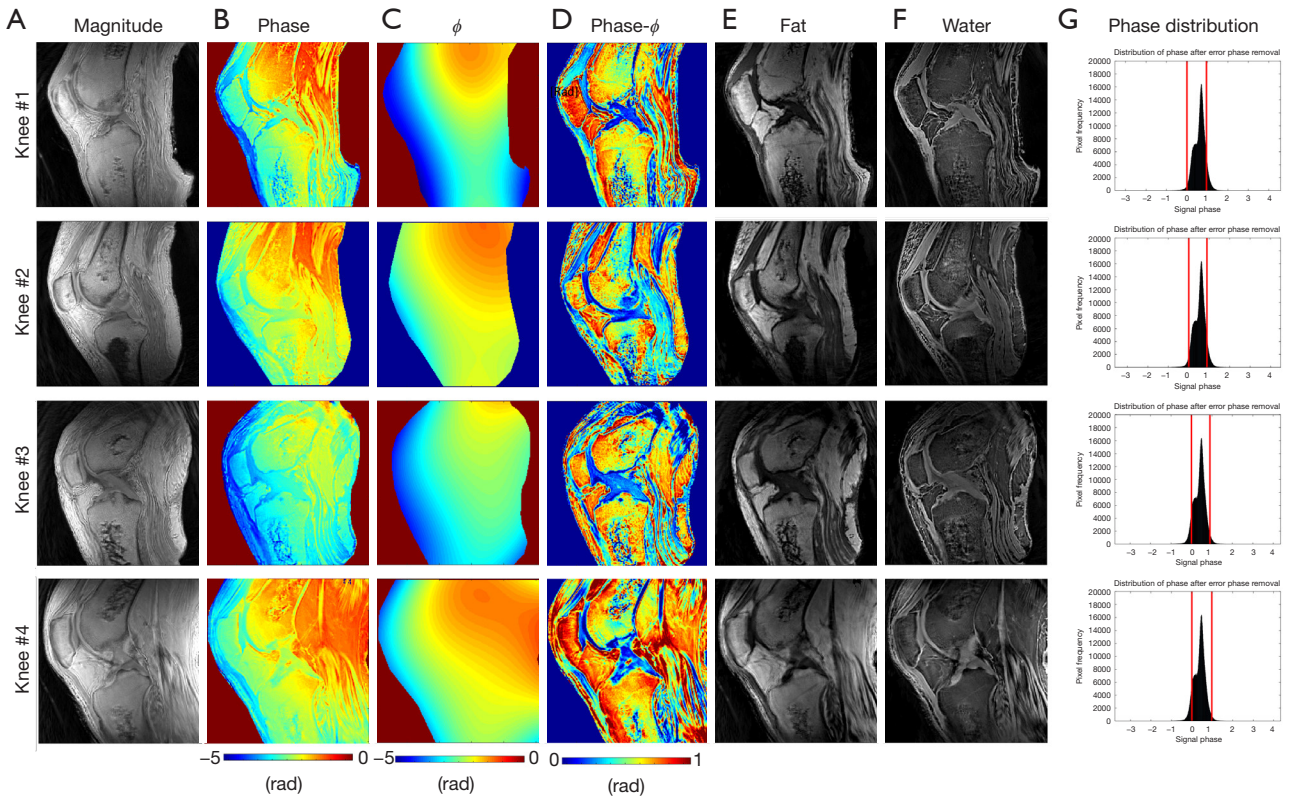

Figure 5 *Ex vivo* experiment with four cadaveric knee joints. (A) Magnitude and (B) phase of the input UTE image; (C) the estimated ϕ map; (D) ϕ-corrected phase image; the resultant (E) fat and (F) water images from the proposed 1p-Dixon; (G) the histogram of phase distribution after ϕ-correction. (G) The left red lines show the estimated water phase, while the right red lines represent the estimated fat phase, $\theta(TE)$. In the estimated water image (i.e., fat-suppressed image), both short and long T2 tissues are clearly delineated, including tendons, ligaments, cartilages, and muscles. 1p-Dixon, single-point Dixon; UTE, ultrashort echo time.

Table 2 CNR of signal magnitude image and estimated water image for patella tendon, cartilage, PCL, ACL, and meniscus in cadaveric knees and healthy volunteers

Subjects	Techniques	Patella tendon	Cartilage	PCL	ACL	Meniscus	P value
Ex vivo (n=4)	No 1p-Dixon	2.7±1.1	3.2±2.3	1.8±1.6	1.1±0.9	4.1±0.8	0.0002
	1p-Dixon	8.1±1.9	9.6±5.0	5.0±1.8	4.5±2.4	3.4±0.5	
In vivo (n=6)	No 1p-Dixon	3.0±2.6	15.4±3.3	4.9±3.0	6.9±6.2	2.7±1.2	<0.0001
	1p-Dixon	23.8±3.2	41.0±9.7	16.4±5.8	22.7±5.5	5.1±6.0	

Data are presented as mean ± standard deviation. 1p-Dixon, single-point Dixon; ACL, anterior cruciate ligament; CNR, contrast-to-noise ratio; PCL, posterior cruciate ligament.

separation of short T2 signal at UTE. However, the water signal detected in muscle using the proposed 1p-Dixon was overall lower than that detected with other methods (green arrows), which may be attributed to imperfect phase modeling or the influence of different water and fat signal intensities at different TEs.

Discussion

Dixon techniques were developed to address partial volume effect arising from the coexistence of fat and water signals within the same voxel. 1p-Dixon utilizes both phase and magnitude information (i.e., the complex signal) to separate

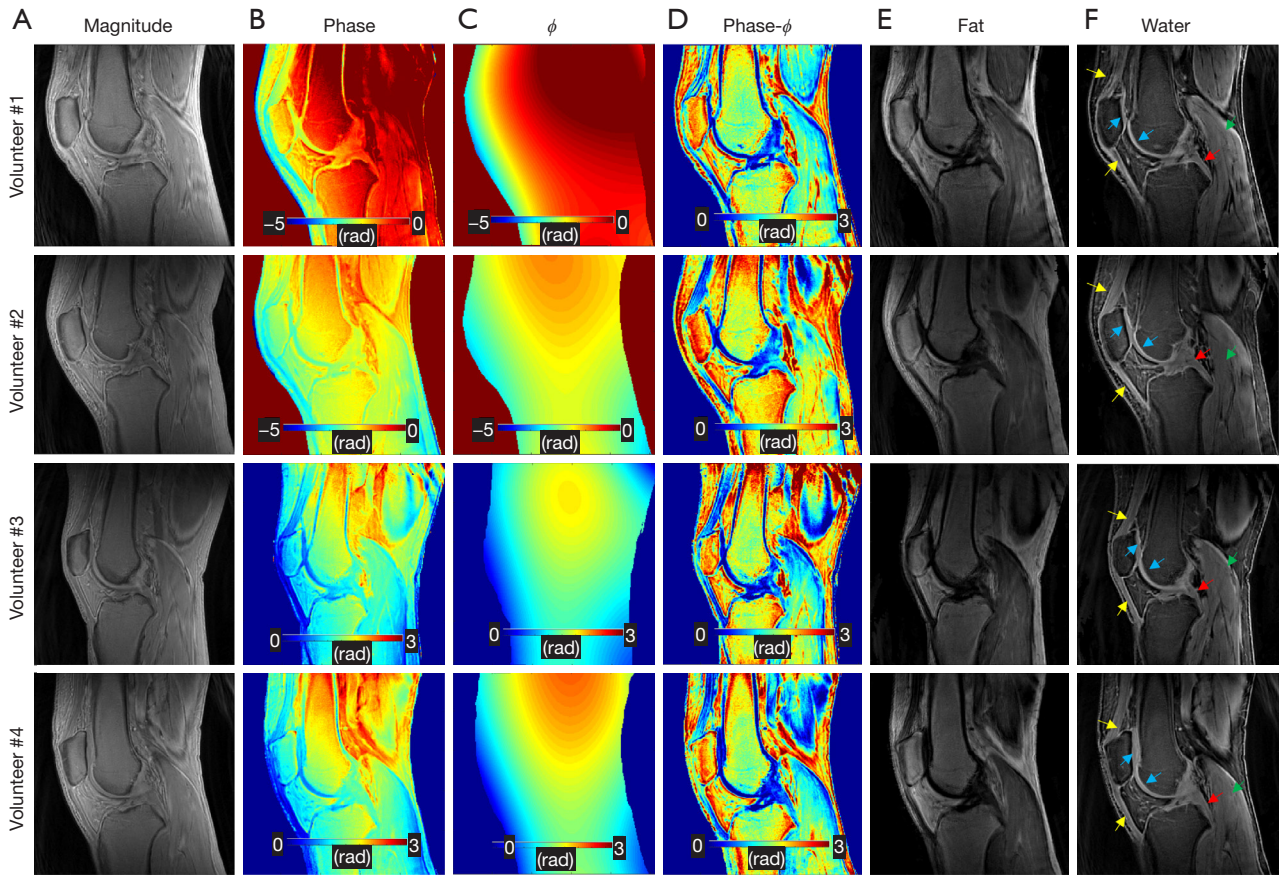

Figure 6 *In vivo* experiment with two healthy volunteers. (A) Magnitude and (B) phase of the input UTE image; (C) the estimated ϕ map; (D) ϕ-corrected phase image; the resultant (E) fat and (F) water images from the proposed 1p-Dixon. (F) The water images show robust fat suppression which exhibits high contrast for the tissues of interest, including tendons (yellow arrows), ligaments (red arrows), muscles (green arrows), and cartilages (blue arrows). 1p-Dixon, single-point Dixon; UTE, ultrashort echo time.

these signals into fat and water components. Since there are two unknowns (fat and water) and a single measurement comprising both real and imaginary components, the estimation of fat and water signals is made possible using Eq. [2] and Eq. [3]. In this study, we demonstrated the feasibility of the proposed 1p-Dixon approach based on a data-driven phase modeling for rapid morphological imaging of short T2 tissues and tested our approach in the human knee, where many different short T2 tissues exist. The proposed method was evaluated with a fat-water phantom, four *ex vivo* cadaveric knee joints, and six *in vivo* human knee joints, showing efficient suppression of fat signal and providing high contrast imaging specific to short T2 tissues. Although we tested this technique only in the knee joint, it can potentially be used in any part of the body, including lungs or brain (7,8).

UTE imaging is a valuable approach to visualizing tissues, which do not show any signal on conventional MRI due to their short T2 values (1,5). For qualitative assessment of those structures, conventional MRI is still useful, as traumatic or degenerative changes are still evaluable. The problem comes with advanced imaging, which includes quantitative assessments of the tissues. UTE imaging plays a crucial role in the quantitative analysis of those short T2 structures that are present all over the body: most parts of the lung tissues (6,27), tendons (28,29), ligaments (30,31), and other structures of the MSK system (32,33), myelin in the brain (9,10,34) or iron (35-37) in tissues when there is an overload, for example.

The proposed approach to model ϕ based on smooth 3D polynomials is highly plausible and feasible, as demonstrated in the *in vitro*, *ex vivo*, and *in vivo*

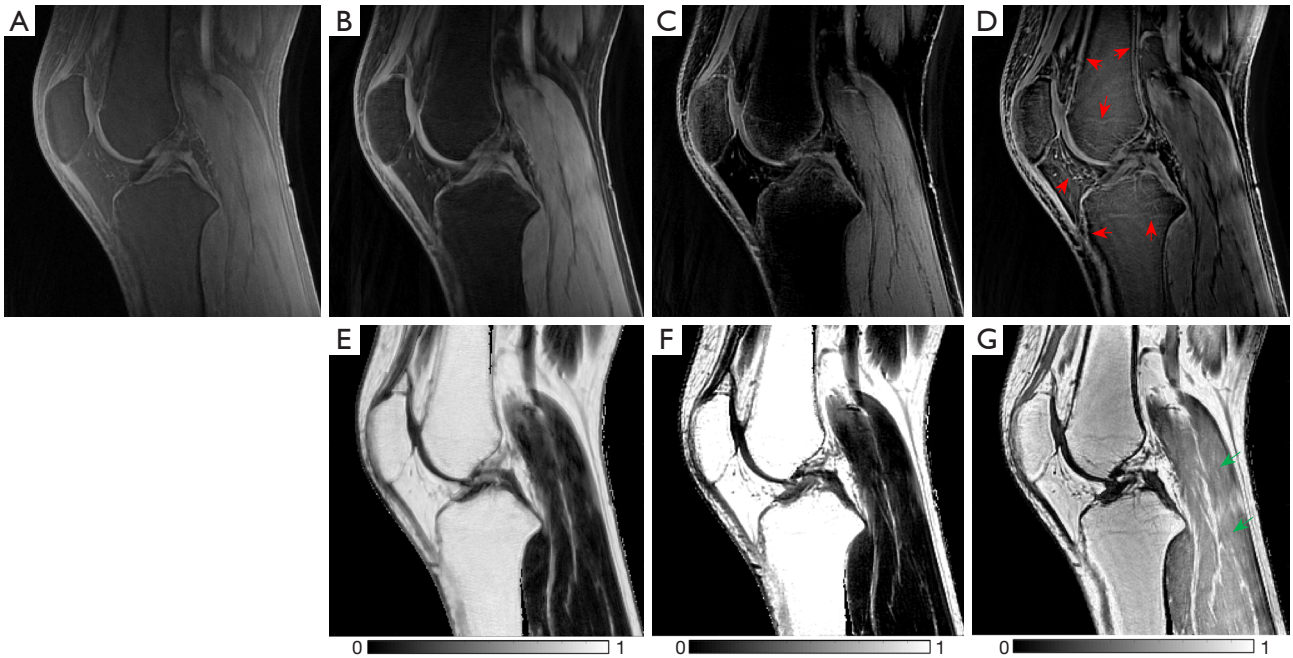

Figure 7 Comparison between different fat suppression techniques. The water image from (A) fat-saturation, (B) 2p-Dixon, (C) conventional 1p-Dixon, and (D) 1p-Dixon with phase modeling; the resultant fat fraction from (E) 2p-Dixon, (F) conventional 1p-Dixon, and (G) 1p-Dixon with phase modeling. The proposed 1p-Dixon with phase modeling demonstrates superior delineation of small structures within short T2 tissues compared to the other methods (red arrows). However, the water signal observed in muscle using this method is generally lower than that detected with other techniques (green arrows). 1p-Dixon, single-point Dixon; 2p-Dixon, two-point Dixon; UTE, ultrashort echo time.

experiments. This approach assumes that the initial phase offset (i.e., B1 phase) and the phase terms induced by B0 inhomogeneity are smooth. The B1 phase is known to result from the double integral of electrical conductivity in the spatial domain, and as such, it is expected to be spatially smooth (38). Additionally, the phase error induced by B0 inhomogeneity is negligibly small and remains smooth in the spatial domain at ultrashort TE (18). A downside of this simple approach is that an additive constant phase offset, which is often observed presumably due to imperfection in data readout and image reconstruction, cannot be removed because it only filters out high-frequency components of the phase image. In addition, the accuracy of 1p-Dixon directly relies on the estimation of the chemical shift-induced phase evolution, $\theta(TE)$, which is directly related to an effective TE that is influenced by several different factors, such as radiofrequency (RF) pulse, readout scheme, and MR system imperfection, causing timing errors. It is, therefore, difficult to accurately estimate $\theta(TE)$ either analytically or empirically.

The proposed histogram-based approach may provide a fast and simple way to estimate the constant phase offset and $\theta(TE)$ without additional scan or priori-known information. In the proposed approach, the phase value in the bottom 2.5% of the phase distribution was used as a reference to remove the constant phase offset, while the phase value in the top 2.5% of the phase distribution was used as a reference for $\theta(TE)$. However, there may be an error in the estimated $\theta(TE)$ with images containing voxels that have a low SNR. To mitigate this error, more advanced masking techniques are desirable that can exclude noisy data in the histogram. Further investigation into this will be performed with a larger number of subjects in our future studies.

Additionally, in the routine clinical setting, time pressure exists, which makes advancements in the development of time-saving MRI methods and techniques necessary. Because the proposed 1p-Dixon method utilizes intrinsic information derived from the single UTE signal, it imposes a shorter scan time than the mp-Dixon approach, which requires repeated acquisitions of images at different TEs. Moreover, 1p-Dixon directly decomposes a single UTE signal into the fat and water signals at the targeted TE,

which likely gives a more accurate snapshot of the signal at the TE than conventional 2p-Dixon. The fat and water signals estimated by 2p-Dixon may not reflect the actual signal at the TE if there is significant T2* decay between the two TEs used in the Dixon algorithm, a principle also demonstrated in our previous work (10). Therefore, our 1p-Dixon approach poses a time-saving and robust alternative to existing fat suppression techniques in UTE imaging.

This study has several limitations. First, only a limited number of healthy volunteers were scanned. Second, only a simple morphological UTE imaging has been investigated in this feasibility study. Third, only knee joints have been demonstrated, although the proposed technique is capable of imaging other body parts. Fourth, although we demonstrated fat-fraction estimation using the fat phantom, the proposed approach may not yield accurate proton density fat fraction (PDFF) measurements due to various factors, such as T1 weighting of the fat/water signal, low SNR, and residual errors in data processing, which requires further investigation. Future studies should test the proposed techniques in different UTE sequences, including UTE magnetization transfer (UTE-MT) (21), UTE double echo steady state (UTE-DESS) (23,24), and UTE-T1 mapping (25), in a larger cohort of human subjects including patients with MSK disorders. Also, future studies should add many more body compartments, such as the spine, pelvis, ankle, and elbow, and evaluate the feasibility of our findings.

Conclusions

In this study, we demonstrated the feasibility of 1p-Dixon-based fat suppression for UTE imaging on a 3T clinical MR system. The UTE 1p-Dixon method, based on the proposed data-driven phase modeling, provides fast and robust fat suppression for UTE imaging without requiring additional data acquisition or prior knowledge, which may facilitate the clinical translation of UTE imaging.

Acknowledgments

None.

Footnote

Reporting Checklist: The authors have completed the STROBE reporting checklist. Available at https://qims.amegroups.com/article/view/10.21037/qims-24-1998/rc

Funding: This study was supported by the National Institutes of Health (NIH) [Nos. R01AR078877 (to H.J.), R01AR075825 to (E.Y.C.), R01AR062581, R01AR068987, and RF1AG075717 (to J.D.), R01AR079484 and R21AR075851 (to Y.M.), and K01AR080257 (to S.J.)], the Deutsche Forschungsgemeinschaft (DFG) [No. SE3272/1-1 (to S.S.)], the University Heidelberg Project Expanding Internationality (to S.S.), the Veterans Affairs Clinical Science Research and Development [Merit Awards I01CX002211 (to J.D.), and I01CX001388 and I01RX002604 (to E.Y.C.)], and GE Healthcare with research support (to H.J., E.Y.C., J.D., and Y.M.).

Conflicts of Interest: All authors have completed the ICMJE uniform disclosure form (available at https://qims.amegroups.com/article/view/10.21037/qims-24-1998/coif). J.D. serves as an unpaid Editorial Board Member of *Quantitative Imaging in Medicine and Surgery*. M.C. reports that he was the employee of GE Healthcare during the study. H.J. received funding from the National Institutes of Health (NIH) (No. R01AR078877). E.Y.C. received funding from the NIH (No. R01AR075825). J.D. received funding from the NIH (Nos. R01AR062581, R01AR068987, and RF1AG075717). Y.M. received funding from the NIH (Nos. R01AR079484 and R21AR075851). H.J., E.Y.C., J.D., and Y.M. received research support from GE Healthcare. S.S. received funding from the Deutsche Forschungsgemeinschaft (DFG) (No. SE3272/1-1) and the University Heidelberg Project Expanding Internationality. E.Y.C. received funding from the Veterans Affairs Clinical Science Research and Development (Merit Awards I01CX001388 and I01RX002604). J.D. received funding from the Veterans Affairs Clinical Science Research and Development (Merit Award I01CX002211). The other authors have no conflicts of interest to declare.

Ethical Statement: The authors are accountable for all aspects of the work in ensuring that questions related to the accuracy or integrity of any part of the work are appropriately investigated and resolved. The study was conducted in accordance with the Declaration of Helsinki (as revised in 2013). The study was approved by Human Research Protections Program (HRPP) of the University of California, San Diego (No. 201909). Written informed consent was obtained from the study participants.

References

1. Chang EY, Du J, Chung CB. UTE imaging in the musculoskeletal system. J Magn Reson Imaging 2015;41:870-83.
2. Afsahi AM, Sedaghat S, Moazamian D, Afsahi G, Athertya JS, Jang H, Ma YJ. Articular Cartilage Assessment Using Ultrashort Echo Time MRI: A Review. Front Endocrinol (Lausanne) 2022;13:892961.
3. Bae WC, Dwek JR, Znamirowski R, Statum SM, Hermida JC, D'Lima DD, Sah RL, Du J, Chung CB. Ultrashort echo time MR imaging of osteochondral junction of the knee at 3 T: identification of anatomic structures contributing to signal intensity. Radiology 2010;254:837-45.
4. Du J, Bydder GM. Qualitative and quantitative ultrashort-TE MRI of cortical bone. NMR Biomed 2013;26:489-506.
5. Ma Y, Jang H, Jerban S, Chang EY, Chung CB, Bydder GM, Du J. Making the invisible visible-ultrashort echo time magnetic resonance imaging: Technical developments and applications. Appl Phys Rev 2022;9:041303.
6. Takahashi M, Togao O, Obara M, van Cauteren M, Ohno Y, Doi S, Kuro-o M, Malloy C, Hsia CC, Dimitrov I. Ultra-short echo time (UTE) MR imaging of the lung: comparison between normal and emphysematous lungs in mutant mice. J Magn Reson Imaging 2010;32:326-33.
7. Sedaghat S, Jang H, Ma Y, Afsahi AM, Reichardt B, Corey-Bloom J, Du J. Clinical evaluation of white matter lesions on 3D inversion recovery ultrashort echo time MRI in multiple sclerosis. Quant Imaging Med Surg 2023;13:4171-80.
8. Sedaghat S, Jang H, Athertya JS, Groezinger M, Corey-Bloom J, Du J. The signal intensity variation of multiple sclerosis (MS) lesions on magnetic resonance imaging (MRI) as a potential biomarker for patients' disability: A feasibility study. Front Neurosci 2023;17:1145251.
9. Jang H, Ma Y, Searleman AC, Carl M, Corey-Bloom J, Chang EY, Du J. Inversion recovery UTE based volumetric myelin imaging in human brain using interleaved hybrid encoding. Magn Reson Med 2020;83:950-61.
10. Jang H, Wei Z, Wu M, Ma YJ, Chang EY, Corey-Bloom J, Du J. Improved volumetric myelin imaging in human brain using 3D dual echo inversion recovery-prepared UTE with complex echo subtraction. Magn Reson Med 2020;83:1168-177.
11. Haase A, Frahm J, Hänicke W, Matthaei D. 1H NMR chemical shift selective (CHESS) imaging. Phys Med Biol 1985;30:341-4.
12. Krinsky G, Rofsky NM, Weinreb JC. Nonspecificity of short inversion time inversion recovery (STIR) as a technique of fat suppression: pitfalls in image interpretation. AJR Am J Roentgenol 1996;166:523-6.
13. Reeder SB, Pineda AR, Wen Z, Shimakawa A, Yu H, Brittain JH, Gold GE, Beaulieu CH, Pelc NJ. Iterative decomposition of water and fat with echo asymmetry and least-squares estimation (IDEAL): application with fast spin-echo imaging. Magn Reson Med 2005;54:636-44.
14. Eggers H, Brendel B, Duijndam A, Herigault G. Dual-echo Dixon imaging with flexible choice of echo times. Magn Reson Med 2011;65:96-107.
15. Deligianni X, Bär P, Scheffler K, Trattnig S, Bieri O. Water-selective excitation of short T2 species with binomial pulses. Magn Reson Med 2014;72:800-5.
16. Afsahi AM, Ma Y, Jang H, Jerban S, Chung CB, Chang EY, Du J. Ultrashort Echo Time Magnetic Resonance Imaging Techniques: Met and Unmet Needs in Musculoskeletal Imaging. J Magn Reson Imaging 2022;55:1597-612.
17. Carl M, Nazaran A, Bydder GM, Du J. Effects of fat saturation on short T2 quantification. Magn Reson Imaging 2017;43:6-9.
18. Jang H, Carl M, Ma Y, Jerban S, Guo T, Zhao W, Chang EY, Du J. Fat suppression for ultrashort echo time imaging using a single-point Dixon method. NMR Biomed 2019;32:e4069.
19. Jang H, Ma Y, Carl M, Jerban S, Chang EY, Du J. Ultrashort echo time Cones double echo steady state (UTE-Cones-DESS) for rapid morphological imaging of short T2 tissues. Magn Reson Med 2021;86:881-92.
20. Kronthaler S, Boehm C, Feuerriegel G, Börnert P, Katscher U, Weiss K, Makowski MR, Schwaiger BJ, Gersing AS, Karampinos DC. Assessment of vertebral fractures and edema of the thoracolumbar spine based on water-fat and susceptibility-weighted images derived from a single ultra-short echo time scan. Magn Reson Med 2022;87:1771-83.
21. Ma J. A single-point Dixon technique for fat-suppressed fast 3D gradient-echo imaging with a flexible echo time. J Magn Reson Imaging 2008;27:881-90.

22. Carl M, Bydder M, Du J, Takahashi A, Han E. Optimization of RF excitation to maximize signal and T2 contrast of tissues with rapid transverse relaxation. Magn Reson Med 2010;64:481-90.
23. Uecker M, Ong F, Tamir J, Bahri D, Virtue P, Cheng J, Zhang T, Lustig M. Berkeley Advanced reconstruction toolbox. Proc Intl Soc Mag Reson Med 2015;23:2486.
24. Walsh DO, Gmitro AF, Marcellin MW. Adaptive reconstruction of phased array MR imagery. Magn Reson Med 2000;43:682-90.
25. Woolrich MW, Jbabdi S, Patenaude B, Chappell M, Makni S, Behrens T, Beckmann C, Jenkinson M, Smith SM. Bayesian analysis of neuroimaging data in FSL. Neuroimage 2009;45:S173-86.
26. Gurney PT, Hargreaves BA, Nishimura DG. Design and analysis of a practical 3D cones trajectory. Magn Reson Med 2006;55:575-82.
27. Mendes Pereira L, Wech T, Weng AM, Kestler C, Veldhoen S, Bley TA, Köstler H. UTE-SENCEFUL: first results for 3D high-resolution lung ventilation imaging. Magn Reson Med 2019;81:2464-73.
28. Chang EY, Du J, Iwasaki K, Biswas R, Statum S, He Q, Bae WC, Chung CB. Single- and Bi-component T2* analysis of tendon before and during tensile loading, using UTE sequences. J Magn Reson Imaging 2015;42:114-20.
29. Du J, Carl M, Diaz E, Takahashi A, Han E, Szeverenyi NM, Chung CB, Bydder GM. Ultrashort TE T1rho (UTE T1rho) imaging of the Achilles tendon and meniscus. Magn Reson Med 2010;64:834-42.
30. Liu J, Nazaran A, Ma Y, Chen H, Zhu Y, Du J, Li S, Zhou Q, Zhao Y. Single- and Bicomponent Analyses of T2* Relaxation in Knee Tendon and Ligament by Using 3D Ultrashort Echo Time Cones (UTE Cones) Magnetic Resonance Imaging. Biomed Res Int 2019;2019:8597423.
31. Jang H, McMillan AB, Ma Y, Jerban S, Chang EY, Du J, Kijowski R. Rapid single scan ramped hybrid-encoding for bicomponent T2* mapping in a human knee joint: A feasibility study. NMR Biomed 2020;33:e4391.
32. Chu CR, Williams AA, West RV, Qian Y, Fu FH, Do BH, Bruno S. Quantitative Magnetic Resonance Imaging UTE-T2* Mapping of Cartilage and Meniscus Healing After Anatomic Anterior Cruciate Ligament Reconstruction. Am J Sports Med 2014;42:1847-56.
33. Williams A, Qian Y, Golla S, Chu CR. UTE-T2* mapping detects sub-clinical meniscus injury after anterior cruciate ligament tear. Osteoarthritis Cartilage 2012;20:486-94.
34. Ma YJ, Jang H, Chang EY, Hiniker A, Head BP, Lee RR, Corey-Bloom J, Bydder GM, Du J. Ultrashort echo time (UTE) magnetic resonance imaging of myelin: technical developments and challenges. Quant Imaging Med Surg 2020;10:1186-203.
35. von Drygalski A, Moore RE, Nguyen S, Barnes RFW, Volland LM, Hughes TH, Du J, Chang EY. Advanced Hemophilic Arthropathy: Sensitivity of Soft Tissue Discrimination With Musculoskeletal Ultrasound. J Ultrasound Med 2018;37:1945-56.
36. Jang H, von Drygalski A, Wong J, Zhou JY, Aguero P, Lu X, Cheng X, Ball ST, Ma Y, Chang EY, Du J. Ultrashort echo time quantitative susceptibility mapping (UTE-QSM) for detection of hemosiderin deposition in hemophilic arthropathy: A feasibility study. Magn Reson Med 2020;84:3246-55.
37. Lu X, Jang H, Ma Y, Jerban S, Chang EY, Du J. Ultrashort Echo Time Quantitative Susceptibility Mapping (UTE-QSM) of Highly Concentrated Magnetic Nanoparticles: A Comparison Study about Different Sampling Strategies. Molecules 2019;24:1143.
38. Katscher U, Kim DH, Seo JK. Recent progress and future challenges in MR electric properties tomography. Comput Math Methods Med 2013;2013:546562.

Cite this article as: Newbury N, Sedaghat S, Athertya JS, Shin SH, Ma Y, Jerban S, Carl M, Silva ML, Chang EY, Du J, Jang H. Novel fat suppression technique for ultrashort echo time MRI using single-point Dixon phase modeling. Quant Imaging Med Surg 2025;15(5):4580-4591. doi: 10.21037/qims-24-1998

